Photoinduced Electron Transfer in Porphyrin-Oligothiophene-Fullerene Linked Triads by Excitation of a Porphyrin Moiety

Takumi Nakamura,[†] Mamoru Fujitsuka,[†,§] Yasuyuki Araki, Osamu Ito,*[,†] Junya Ikemoto,[‡] Kazuo Takimiya,[‡] Yoshio Aso,[‡,§] and Tetsuo Otsubo*[,‡]

Institute of Multidisciplinary Research for Advanced Materials, Tohoku University, CREST, Japan Science and Technology Agency, Katahira, Sendai, Miyagi 980-8577, Japan, and the Department of Applied Chemistry, Graduate School of Engineering, Hiroshima University, Higashi-Hiroshima 739-8527, Japan

Received: February 27, 2004; In Final Form: May 7, 2004

Photoinduced charge-separation (CS) and recombination (CR) processes of porphyrin (H_2P)-oligothiophene (*n*T)-fullerene (C_{60}) linked triads (H_2P-*n*T-C_{60}, $n = 4$, 8, and 12), which were designed to reveal the function of *n*T as a molecular wire for the electron-transfer (ET) process, have been investigated by time-resolved fluorescence and absorption spectroscopic methods. After the excitation of the H_2P moiety in toluene, ^1H_2P*-*n*T-C_{60} showed predominantly the energy-transfer (EN) process generating H_2P-*n*T-$^1C_{60}$*, whereas the CS process was not observed. The EN rate constant depends on the length of *n*T. In benzonitrile (PhCN) and *o*-dichlorobenzene (*o*-DCB), $H_2P^{\cdot+}$-*n*T-$C_{60}^{\cdot-}$ was produced from ^1H_2P*-*n*T-C_{60}. The most energetically stable final CS state was confirmed to be H_2P-*n*T$^{\cdot+}$-$C_{60}^{\cdot-}$, which was produced by the hole-shift process from $H_2P^{\cdot+}$-*n*T-$C_{60}^{\cdot-}$. The rate constant for the CS process from ^1H_2P*-*n*T-C_{60} to $H_2P^{\cdot+}$-*n*T-$C_{60}^{\cdot-}$ decreased with the length of the *n*T moiety, indicating that the *n*T moiety acts as a molecular wire. The small damping factor showed a pronounced solvent polarity effect (0.03 $Å^{-1}$ in PhCN and 0.11 $Å^{-1}$ in *o*-DCB), indicating that a long-range ET process through the *n*T moiety is feasible in polar solvents. The final CS state (H_2P-*n*T$^{\cdot+}$-$C_{60}^{\cdot-}$) returned to a neutral triad by the CR process between the vicinal electron (radical anion) and hole (radical cation). The lifetime of the CS state showed the solvent polarity effect ranging from 1.5−2.4 μs in PhCN to 14−27 μs in *o*-DCB at room temperature. The longest lifetime (27 μs) was observed with H_2P-8T$^{\cdot+}$-$C_{60}^{\cdot-}$ in *o*-DCB. From the temperature dependence of the CR rate constant, the reorganization energies were evaluated to be 0.8−1.1 eV for all triads in PhCN and *o*-DCB.

Introduction

Conjugated nanoscale molecules are useful for the molecular electronic devices such as EL devices,[1] photovoltaic cells,[2] field-effect transistors,[3] nonlinear optics,[4] and electrical conductors.[5] Recently, photoinduced electron-transfer systems with highly efficient charge-separation (CS) and slow charge-recombination (CR) processes have been applied to photovoltaic cells.[2] Highly conjugated nanoscale molecular wires are indispensable for single-molecule electron devices.[5] Oligothiophenes (*n*T's) seem to be one of the most well-investigated oligomers of π-conjugated polymers[6−8] because of remarkable characteristics of *n*T's such as a rigid rodlike structure and a highly delocalized π conjugation. These *n*T's with high π conjugation are expected to serve as molecular wires for electron transfer (ET) and energy transfer (EN). In general, the photoinduced CS process is mainly influenced by redox properties of the acceptor and donor, the reorganization energy, and the distance between the acceptor and donor moieties.[9−19]

Recently, fullerene C_{60} has been employed as an electron acceptor of the electron-transfer systems because of its unique characteristics;[20] an energy gap of about 1.8 eV separates a 3-fold degenerate LUMO from a lower-lying 5-fold degenerate HOMO in C_{60}, which is advantageous to attain the appropriate driving force for the CS process via the excited state.[21] One of the other remarkable properties of C_{60} is a low reduction potential (−0.51 V vs SCE, in benzonitrile (PhCN)), affording a good electron-acceptor ability.[22,23] Furthermore, another important characteristic of C_{60} is a low reorganization energy in the electron-transfer processes.[15−18,24] Several research groups have reported photophysical and photochemical properties of fullerene-donor linked dyad molecules;[25−41] for example, aniline-C_{60},[25] carotenoid-C_{60},[26] ferrocene-C_{60},[27] oligothiophene-C_{60},[28] porphyrin-C_{60},[29−33] pyrazine-C_{60} dyad molecules,[34] and so forth.[35−41]

We recently reported that *n*T's mixed with fullerene (C_{60} or C_{70}) donate an electron to the triplet excited state of fullerene via the intermolecular ET process in polar solvents.[42] More recently, efficient CS processes were reported to occur in oligothiophene-C_{60} dyads.[6,28] The lifetimes of the CS states of *n*T-C_{60} dyads were on the order of 10^{-6}−10^{-5} s in polar solvents. It is interesting that the lifetime of the CS state becomes longer for shorter *n*T's with a large negative free-energy change (ΔG) for the CR process because the CR processes of these dyads are in the Marcus inverted region.[43] Furthermore, the CS processes occurred not only in solution but also in fine particles.[28c] It was also reported that the self-assembled monolayers of these dyads show photovoltaic effects.[6]

In the present study, we examined the CS and CR processes as well as the EN process in porhyrin-oligothiophene-C_{60} triads (H_2P-*n*T-C_{60} (H_2P = triphenylporphyrin in Figure 1)), where

* Corresponding authors. (O.I.) E-mail: ito@tagen.tohoku.ac.jp. (T.O.) otsubo@hiroshima-u.ac.jp.
† Tohoku University.
‡ Hiroshima University.
§ Present address: The Institute of Scientific and Industrial Research, Osaka University, Ibaraki, Osaka 567-0047, Japan.

10.1021/jp049122u CCC: $27.50
Published on Web 06/22/2004

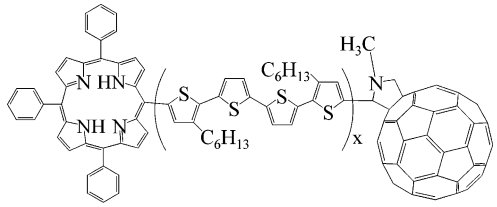

H_2P-*n*T-C_{60} (x = 1, 2, and 3; n = 4, 8, and 12)

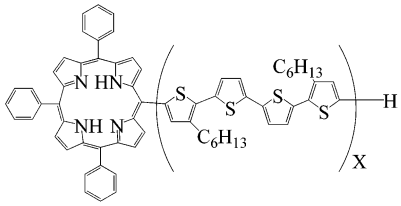

H_2P-*n*T (x = 1, 2, and 3; n = 4, 8, and 12)

Figure 1. Molecular structures of H_2P-*n*T-C_{60} and H_2P-*n*T.

H_2P was employed as an antenna molecule harvesting photons in a wide wavelength region because the H_2P moiety can absorb visible light more efficiently than the *n*T-C_{60} dyads. In these triads, the multifunctional roles of *n*T's as a molecular spacer for EN and as a molecular wire for ET were revealed by the time-resolved absorption and fluorescence measurements. To investigate the distance dependence of *n*T on the efficiencies of the CS and EN processes, we compared three triads by varying the length of *n*T ($n = 4$, 8, and 12). The alkyl groups were introduced as substituents at the β positions of the thiophene rings to obtain a higher solubility of dyad and triad molecules in organic solvents.

Experimental Section

Materials. Syntheses of H_2P-*n*T and H_2P-*n*T-C_{60} were described in the previous paper.[44] Components such as *n*T ($n = 4$, 8, and 12) and *N*-methylpyrrolidino-C_{60} ($NMPC_{60}$) were prepared according to the methods described in the literature.[22a] Other chemicals such as tetraphenylporphyrin (H_2TPP) and solvents (benzonitrile (PhCN), *o*-dichlorobenzene (*o*-DCB), and toluene) were of the best commercial grade available.

Methods. Steady-state absorption spectra were measured on a JASCO V-530 UV−vis spectrophotometer. Steady-state fluorescence spectra were measured on a Shimadzu RF-5300 PC spectrofluorophotometer.

The fluorescence lifetimes were measured by a single-photon counting method with a streak scope (Hamamatsu Photonics, C4334−01) using the second harmonic generation (SHG, 410 nm) of a Ti:sapphire laser (Spectra-Physics, Tsunami 3950-L2S, fwhm 1.5 ps) as an excitation source.

The nanosecond transient absorption spectra were measured using the pulsed laser light from an optical parametric oscillation (Continuum, Surelite OPO, fwhm 4 ns) pumped by an Nd:YAG laser (Continuun, Surelite II-10). For the measurements of the transient absorption spectra in the near-IR region, we used a Ge avalanche photodiode (APD, Hamamatsu Photonics, B2834) as a detector for monitoring light from the pulsed xenon lamp.

The picosecond transient absorption spectra were measured by the pump and probe method using a Ti:sapphire regenerative amplifier seeded by the SHG of an Er-doped fiber laser (Clark-MXR CPA-2001 plus, 1 kHz, fwhm 150 fs). A white continuum pulse light used as a probe light was generated by focusing the fundamental of the amplifier on a rotating H_2O cell. The samples were excited by the pulsed laser light from the SHG (388 nm) of fundamentals or output of OPA (Clark-MXR vis-OPA, 560 nm). The probe light that transmitted through the sample in a rotating cell was detected with a dual MOS detector (Hamamatsu Photonics, C6140) for the visible region or an InGaAs linear image sensor (Hamamatsu Photonics, C5890-128) for the near-IR region.

TABLE 1: Redox Potentials in *o*-DCB[a]

	E/V (vs $Fc/Fc^{\cdot+}$)				
materials	$H_2P/H_2P^{\cdot+}$	$nT/nT^{\cdot+}$	$C_{60}/C_{60}^{\cdot-}$	$H_2P/H_2P^{\cdot-}$	$nT/nT^{\cdot-}$
H_2P-4T	0.66	0.45		−1.56	−1.59
H_2P-4T-C_{60}	0.68	0.43	−1.20	−1.58	−1.58
H_2P-8T	0.55	0.32		−1.60	−1.58
H_2P-8T-C_{60}	0.56	0.29	−1.20	−1.60	−1.58
H_2P-12T	0.48	0.22		−1.62	−1.56
H_2P-12T-C_{60}	0.49	0.21	−1.19	−1.62	−1.56
H_2TPP	0.53			−1.54	
4T		0.50			−1.59
8T		0.34			−1.58
12T		0.19			-1.52
$NMPC_{60}$			−1.18		

[a] Square wave voltammetric measurements were carried out with a potentiostat and a cell equipped with a platinum working electrode, an Ag/Ag^+ reference electrode, and a platinum counter electrode in *o*-DCB containing 0.10 M tetra-*n*-butylammonium hexafluorophosphate at room temperature.

Square wave volumetric measurements were carried out with a potentiostat (BAS CV50W) and a cell equipped with a platinum working electrode, an Ag/Ag^+ reference electrode, and a platinum counter electrode. All electrochemical measurements were performed in *o*-DCB containing 0.10 M tetra-*n*-butylammonium hexafluorophosphate (Nacalai Tesque) at room temperature. The redox potentials were corrected against the ferrocene/ferrocenium (Fc/Fc^+) couple.

Molecular structures were optimized by the MM3 force field modified in MacroModel package, taking the dielectric constants into consideration.

Results and Discussion

Optimized Structures. Figure 2 shows the optimized structures of H_2P-*n*T-C_{60} in polar media, which were calculated by the MM3 force field modified for the MacroModel package, taking the dielectric constant of PhCN ($\epsilon = 25.2$). It is revealed that the rigid *n*T chain stretches in a polar solvent and that the H_2P moiety and the C_{60} moiety are spatially separated. In less polar solvents with small dielectric constants (*o*-DCB ($\epsilon = 9.93$) and toluene (in vacuum)), similar structures were obtained (Supporting Information, Figures S1 and S2).

Steady-State Absorption Spectra. Absorption spectra of H_2P-*n*T-C_{60} and the corresponding components, H_2TPP, *n*T, and $NMPC_{60}$, in PhCN are shown in Figure 3. The B band of the H_2P moiety in H_2P-*n*T-C_{60} shifted slightly to the longer wavelength and became broader than that of H_2TPP, suggesting that the symmetry of the H_2P moiety in H_2P-*n*T-C_{60} becomes lower than that of H_2TPP. These findings indicate a weak interaction between the H_2P and *n*T moieties in H_2P-*n*T-C_{60}. Similar absorption spectra were observed in *o*-DCB and toluene; no appreciable solvent effect was confirmed in the absorption spectra.

Electrochemical Properties and Free-Energy Changes. The redox potentials of H_2P-*n*T-C_{60} measured by square wave voltammetry in *o*-DCB are summarized in Table 1. The redox potentials of H_2P-8T-C_{60} (+0.56, +0.29, −1.20 V) and H_2P-12T-C_{60} (+0.49, +0.21, −1.19 V) can be roughly explained on the basis of those of the components, H_2TPP (+0.53 V),

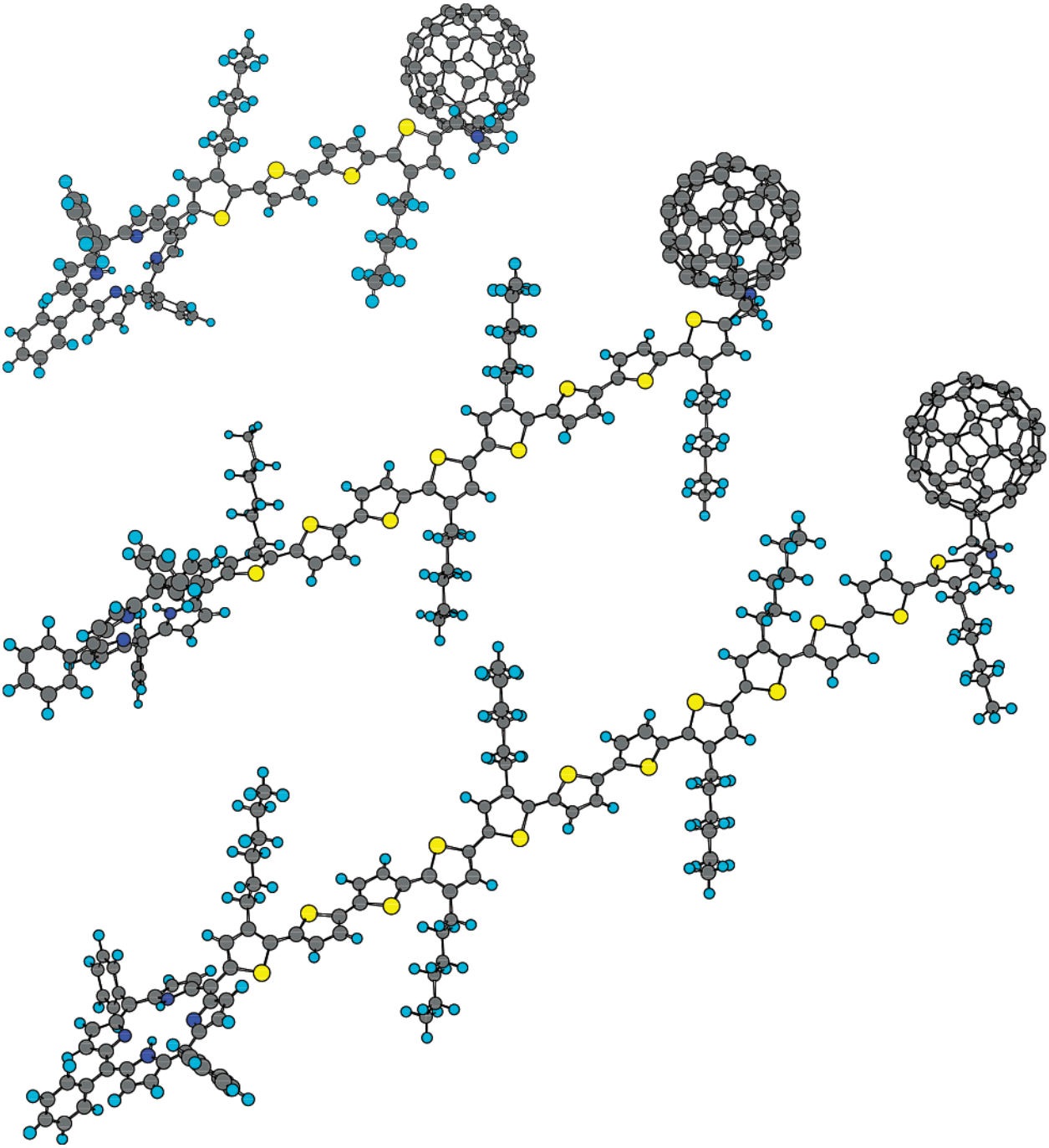

Figure 2. Optimized structures of H_2P-*n*T-C_{60} in a polar solvent ($\epsilon = 25.2$). The structures were calculated by the MM3 method modified for MacroModel.

8T (+0.34 V), 12T (+0.19 V), and NMPC_{60} (−1.18 V), which imply only a weak electronic interaction among the three moieties. In the cases of H_2P-4T-C_{60} (+0.68, +0.43, −1.20 V) and H_2P-4T (+0.66, +0.45 V), an appreciable difference was observed between the H_2P moiety and H_2TPP, which is due to a positive charge on 4T that reduces the electron density of H_2P because the distance between the H_2P moiety and the center of the cation radical of the 4T moiety is shorter than those of H_2P-8T-C_{60} and H_2P-12T-C_{60}.

From the oxidation potentials (E_{ox}) of the H_2P and *n*T moieties, the electron-donor abilities increase in the order of H_2P < 4T < 8T < 12T in the dyads and triads. The reduction potentials (E_{red}) indicate that the electron-acceptor abilities increase in the order of $H_2P \approx n\text{T} \ll C_{60}$.

The ΔG values for the CS ($-\Delta G_{CS}$) and CR processes ($-\Delta G_{CR}$) in toluene, *o*-DCB, and PhCN were calculated using Weller's equation (eqs 1 and 2):[45,46]

$$-\Delta G_{CR} = E_{ox} - E_{red} + \Delta G_S \quad (1)$$

$$-\Delta G_{CS} = \Delta E_{0-0} - (-\Delta G_{CR}) \quad (2)$$

where ΔE_{0-0} is referred to the energy of the lowest excited state and ΔG_S is referred to as a static Coulomb interaction calculated by the ordinary method. (See the equation in the footnote of Table S1 in Supporting Information.)[45,46] These ΔG_{CR} values show that the most stable radical-ion pair in the triads is H_2P-*n*T$^{\cdot+}$-$C_{60}^{\cdot-}$ (*n*T = 4T, 8T, and 12T). From these ΔG_{CS} and ΔG_{CR} values, the energy diagram can be drawn as shown

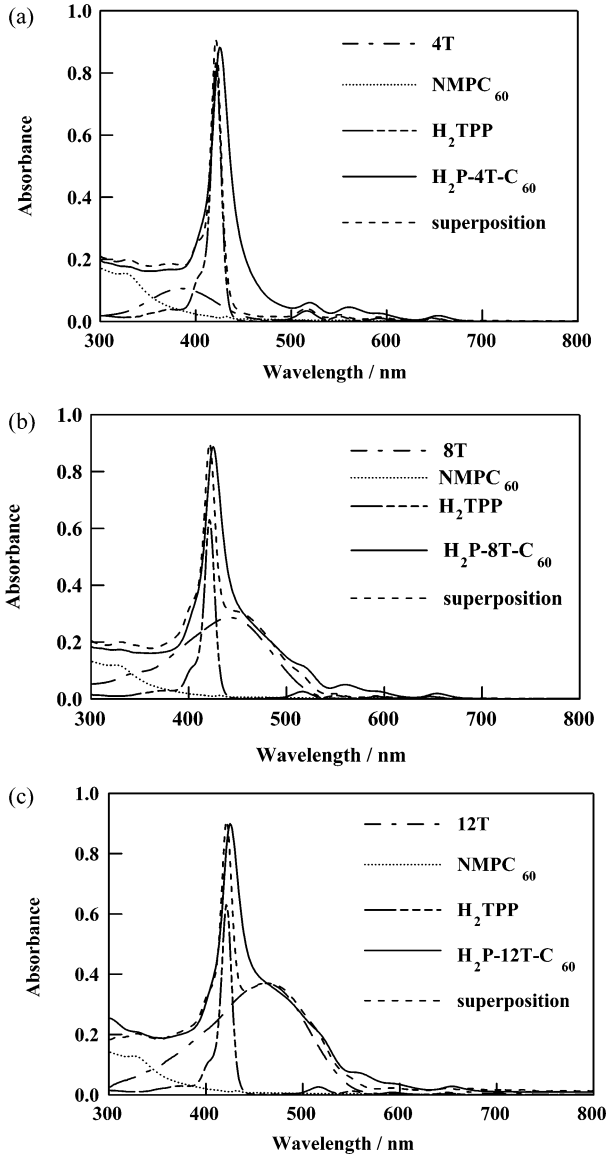

Figure 3. Steady-state absorption spectra of (a) H_2P-4T-C_{60}, (b) H_2P-8T-C_{60}, and (c) H_2P-12T-C_{60} and their components in PhCN.

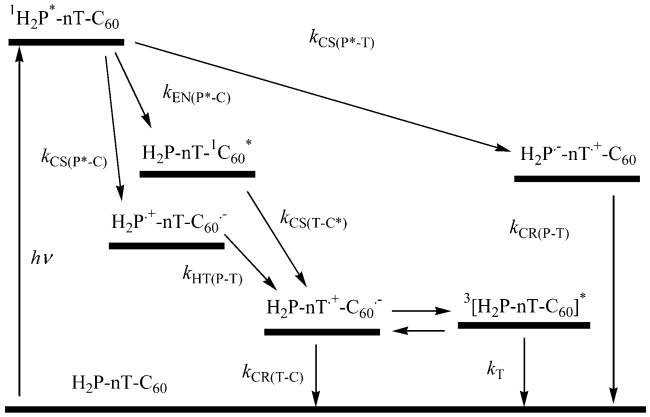

Figure 4. Schematic main processes for H_2P-*n*T-C_{60} in polar solvents, considering driving forces ($-\Delta G_{CS}$ and $-\Delta G_{EN}$) and free energy changes (ΔG_{CR}). Each energy level varies with *n*T and solvent polarity. Because energy levels of ^3H_2P*-*n*T-C_{60} are similar to those of H_2P-*n*T-$^3C_{60}$*, they are described as ^{3}[H_2P-*n*T-C_{60}]*.

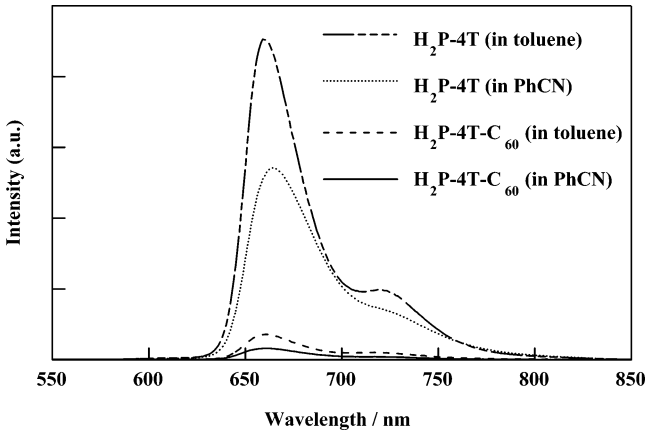

Figure 5. Fluorescence spectra of H_2P-*n*T (in toluene and PhCN) and H_2P-*n*T-C_{60} (in toluene and PhCN). Excitation wavelength is 410 nm. Absorption intensities of the samples were matched at the excitation wavelength.

in Figure 4, in which the energy levels vary with *n*T's and solvent polarity. Possible EN, CS, and CR processes after photoexcitation of the H_2P and *n*T moieties are also shown in Figure 4.

Steady-State Fluorescence Measurement. Figure 5 shows the fluorescence spectra of H_2P-4T-C_{60} and H_2P-4T upon excitation of the H_2P moiety with 410-nm light in PhCN and toluene; the absorption intensities of the samples were matched at the excitation wavelength for the fluorescence measurements. The fluorescence band at 670 nm with a shoulder at about 725 nm of H_2P-4T can be attributed to the ^1H_2P* moiety. Because the fluorescence intensity in PhCN was smaller than that in toluene, the CS process between the H_2P and 4T moieties takes place. From the ΔG_{CS} values, the formation of $H_2P^{\cdot-}$-4T$^{\cdot+}$ via ^1H_2P*-4T is possible in PhCN (Supporting Information, Table S2). For H_2P-4T-C_{60} in toluene, the fluorescence intensity of the ^1H_2P* moiety decreased compared with that of H_2P-4T, suggesting the EN process to the C_{60} moiety in H_2P-4T-C_{60} because the CS process to $H_2P^{\cdot+}$-4T-$C_{60}^{\cdot-}$ via ^1H_2P*-4T-C_{60} is not possible because of the positive ΔG_{CS} value in toluene (Supporting Information, Table S1). In PhCN, a further decrease in the fluorescence intensity was observed compared with that in toluene, suggesting the CS process to $H_2P^{\cdot+}$-4T-$C_{60}^{\cdot-}$ via ^1H_2P*-4T-C_{60} in addition to the EN process. Such a CS process to $H_2P^{\cdot+}$-4T-$C_{60}^{\cdot-}$ via ^1H_2P*-4T-C_{60} is possible because of the negative ΔG_{CS} value in PhCN (Supporting Information, Table S1). In *o*-DCB, similar fluorescence quenching behavior was observed, indicating that both the CS and EN processes take place. For H_2P-*n*T and H_2P-*n*T-C_{60} (n = 8 and 12), similar tendencies to H_2P-4T and H_2P-4T-C_{60} were observed in toluene and PhCN, although it was revealed that the differences depend on the length of the *n*T moiety.

Time-Resolved Fluorescence Measurement in Toluene. Figure 6 shows the fluorescence temporal profiles of H_2P-4T and H_2P-4T-C_{60} after the excitation of the H_2P moiety in toluene and PhCN; for H_2P-*n*T and H_2P-*n*T-C_{60} (n = 8 and 12), similar fluorescence temporal profiles were observed. The profile of ^1H_2P*-*n*T can be fit with a single exponential from which the fluorescence lifetime (τ_F) of the ^1H_2P* moiety was evaluated to be 3.9 ns. Because the τ_F (toluene) values for ^1H_2P*-*n*T are independent of the *n*T moieties (Table 2), this value (3.9 ns) is a characteristic fluorescence lifetime (τ_0) of the H_2P moiety without the ET and EN processes in the dyads. Thus, τ_0^{-1} is

TABLE 2: Fluorescence Lifetimes (τ_F), Quenching Rate Constants (k_q),[a] and Quantum Yields (Φ_q)[a]

	toluene ($\epsilon = 2.38$)			*o*-DCB ($\epsilon = 9.93$)			PhCN ($\epsilon = 25.2$)		
materials	τ_F (ns)	k_q (s^{-1})	Φ_q	τ_F (ns)	k_q (s^{-1})	Φ_q	τ_F (ns)	k_q (s^{-1})	Φ_q
H_2P-4T	3.9			3.2	5.6×10^7	0.18	3.3	4.7×10^7	0.17
H_2P-4T-C_{60}	0.26	3.6×10^9	0.94	0.21	4.5×10^9	0.95	0.18	5.3×10^9	0.95
H_2P-8T	3.9			2.9	8.8×10^7	0.26	1.4	4.6×10^8	0.64
H_2P-8T-C_{60}	2.8	1.0×10^8	0.28	1.7	3.3×10^8	0.56	0.41	2.2×10^9	0.90
H_2P-12T	3.9			2.8	1.0×10^8	0.28	1.3	5.1×10^8	0.66
H_2P-12T-C_{60}	3.7	1.4×10^7	0.04	2.6	1.3×10^8	0.34	0.68	1.2×10^9	0.82

[a] The k_q and Φ_q values were calculated from eqs 3 and 4.

TABLE 3: Rate Constants ($k_{EN(P^*-C)}$) and Quantum Yields ($\Phi_{EN(P^*-C)}$) for Energy Transfer of H_2P-*n*T-C_{60} in Toluene, PhCN, and *o*-DCB

solvent	initial state[a]	final state[a]	$k_{EN(P^*-C)}$ ($\Phi_{EN(P^*-C)}$)	$n = 4$ k (s^{-1})	$n = 8$ k (s^{-1})	$n = 12$ k (s^{-1})
toluene, PhCN, *o*-DCB	$^1H_2P^*$-*n*T-C_{60}	H_2P-*n*T-$^1C_{60}$*	$k_{EN(P^*-C)}$[b]	3.6×10^9	1.0×10^8	1.4×10^7
toluene			($\Phi_{EN(P^*-C)}$)[c]	(0.94)	(0.28)	(0.04)
PhCN			($\Phi_{EN(P^*-C)}$)[d]	(0.65)	(0.04)	(0.01)
o-DCB			($\Phi_{EN(P^*-C)}$)[d]	(0.76)	(0.17)	(0.04)

[a] The energy difference between $^1H_2P^*$ to $^1C_{60}$* was evaluated to be 0.13 eV from the fluorescence bands. [b] The values of $k_{EN(P^*-C)}$ were estimated from the fluorescence quenching rates of $^1H_2P^*$-*n*T-C_{60} in toluene from eq 4 assuming that the k_{EN} values in toluene are the same as in polar solvents. [c] The values of $\Phi_{EN(P^*-C)}$ in toluene were evaluated from eq 4. [d] The values of $\Phi_{EN(P^*-C)}$ in polar solvents were evaluated from eq 6.

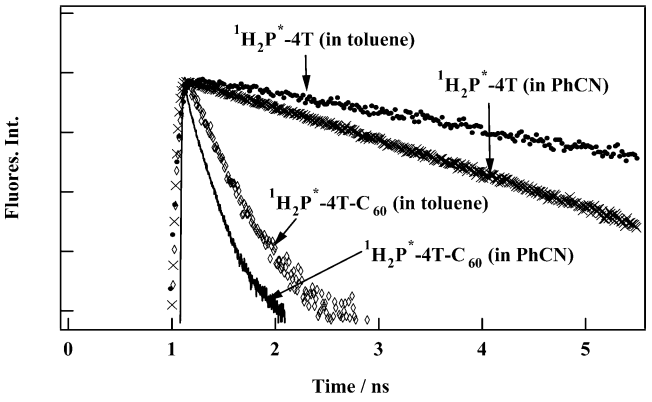

Figure 6. Fluorescence time profiles of H_2P-*n*T and H_2P-*n*T-C_{60} in the 680−720 nm region in toluene and PhCN. Excitation wavelength is 410 nm.

defined as k_d, where $k_d = (k_{ic} + k_{rad} + k_{isc})$ and k_{ic}, k_{rad}, and k_{isc} are the rate constants for the internal conversion, radiative, and intersystem crossing processes (ISC), respectively. In the case of $^1H_2P^*$-4T-C_{60}, fluorescence intensity decreased with time according to a single-exponential function, although a relatively small fraction (10−20%) needed the additional function. From the main decay part, a shorter lifetime than that of $^1H_2P^*$-4T was calculated, corresponding to the appreciable decrease in the steady-state fluorescence intensity. The τ_F values of $^1H_2P^*$-*n*T-C_{60} varied from 0.26 to 3.7 ns depending on the *n*T's as listed in Table 2. On the basis of the τ_0 value, the rate constants (k_q) and quantum yields (Φ_q) for the fluorescence quenching processes were calculated from the observed τ_F values using eqs 3 and 4, respectively, as summarized in Table 2.

$$k_q = \tau_F^{-1} - \tau_0^{-1} \quad (3)$$

$$\Phi_q = \frac{(\tau_F^{-1} - \tau_0^{-1})}{\tau_F^{-1}} \quad (4)$$

The short τ_F values of the triads indicate that the EN process takes place from $^1H_2P^*$-*n*T-C_{60}, producing H_2P-*n*T-$^1C_{60}$* through the *n*T moieties as in eq 5.

$$^1H_2P^*\text{-}n\text{T-}C_{60} \xrightarrow{k_{EN(P^*-C)}} H_2P\text{-}n\text{T-}^1C_{60}^* \quad (5)$$

The k_q and Φ_q values for H_2P-*n*T-C_{60} in toluene are attributed to the rate constants ($k_{EN(P^*-C)}$) and the quantum yields ($\Phi_{EN(P^*-C)}$) for the EN processes (eq 5). Both $k_{EN(P^*-C)}$ and $\Phi_{EN(P^*-C)}$ values drastically decreased from 3.6×10^9 to 1.4×10^7 s^{-1} and from 0.94 to 0.04, respectively, by changing from 4T to 12T (Table 3). Thus, the *n*T moiety acts as a spacer for EN. Because the dependence of $k_{EN(P^*-C)}$ on $1/(R_{DA})^6$ was confirmed, the Förster mechanism is indicated for the present EN process, in which long-range EN was confirmed (R_{DA} = ca. 55.7 Å for H_2P-12T-C_{60}).[47,48] Indeed, the k_{EN} values calculated from the Förster theory are comparable with the observed $k_{EN(P^*-C)}$ values. (Supporting Information, Figure S2). However, the EN process driven by the Dexter mechanism, which is operative in the short-distance EN process, does not operate to 55.7 Å.[49,50]

Time-Resolved Fluorescence Measurements in PhCN and *o*-DCB. In PhCN (Figure 6), a slightly short τ_F value (3.3 ns) of $^1H_2P^*$-4T was observed corresponding to the decrease in the fluorescence intensity compared with that in toluene. According to the Förster theory, the k_{EN} value depends on the refractive index of the solvent; however, the difference in the refractive indexes is quite small (1.497, 1.528, and 1.552 for toluene, PhCN, and *o*-DCB, respectively). Thus, the $k_{EN(P^*-C)}$ values may be nearly the same in these three solvents. As shown in Table 2, the τ_F values of $^1H_2P^*$-*n*T-C_{60} in polar solvents are shorter than those in toluene, suggesting the presence of processes other than EN; thus, the $\Phi_{EN(P^*-C)}$ values in polar solvents must be decreased by such a competitive process as calculated by eq 6.

$$\Phi_{EN(P^*-C)} = \frac{k_{EN(P^*-C)}}{\tau_F^{-1}\ (\text{polar solvent})} \quad (6)$$

TABLE 4: Driving Forces (ΔG_{CS} and ΔG_{HS})[a] and Rate Constants ($k_{CS(P^*-C)}$ and $k_{HS(P-T)}$) of H_2P-*n*T-C_{60} in PhCN and *o*-DCB

				$n = 4$		$n = 8$		$n = 12$	
solvent	initial state	final state		$-\Delta G$ (eV)	k (s^{-1})	$-\Delta G$ (eV)	k (s^{-1})	$-\Delta G$ (eV)	k (s^{-1})
PhCN	$^1H_2P^*$-*n*T-C_{60}	$H_2P^{\cdot+}$-*n*T-$C_{60}^{\cdot-}$	$(k_{CS(P^*-C)})^b$ $(\Phi_{CS(P^*-C)})^b$	0.14	1.7×10^9 ($\Phi = 0.30$)	0.25	1.6×10^9 ($\Phi = 0.67$)	0.33	6.9×10^8 ($\Phi = 0.47$)
	$H_2P^{\cdot+}$-*n*T-$C_{60}^{\cdot-}$	H_2P-*n*T$^{\cdot+}$-$C_{60}^{\cdot-}$	$(k_{HS(P-T)})^c$	0.25	3.5×10^7	0.35	7.7×10^7	0.31	7.0×10^7
o-DCB	$^1H_2P^*$-*n*T-C_{60}	$H_2P^{\cdot+}$-*n*T-$C_{60}^{\cdot-}$	$(k_{CS(P^*-C)})^b$ $(\Phi_{CS(P^*-C)})^b$	0.07	8.6×10^8 ($\Phi = 0.18$)	0.17	1.4×10^8 ($\Phi = 0.24$)	0.24	1.3×10^7 ($\Phi = 0.04$)
	$H_2P^{\cdot+}$-*n*T-$C_{60}^{\cdot-}$	H_2P-*n*T$^{\cdot+}$-$C_{60}^{\cdot-}$	$(k_{HS(P-T)})^c$	0.16	1.1×10^7	0.13	4.3×10^7	0.13	8.6×10^6

[a] ΔG_{CS} and ΔG_{HS} were calculated from eqs 1 and 2, in which $-\Delta G_S = (e^2/(4\pi\epsilon_0))[(1/(2R_+) + 1/(2R_-) - 1/R_{DA})/\epsilon_S - (1/(2R_+) + 1/(2R_-))/\epsilon_R]$, where R_+ and R_- are the radii of the cation and anion, respectively (4T (7.5 Å), 8T (14.5 Å), 12T (21.6 Å), H_2P (5.0 Å), and $NMPC_{60}$ (4.2 Å)). R_{DA} is the center-to-center distance between the donor and acceptor (H_2P-4T (12.5 Å), H_2P-8T (20.1 Å), H_2P-12T (27.6 Å), H_2P-4T-C_{60} (25.5 Å), H_2P-8T-C_{60} (40.4 Å), and H_2P-12T-C_{60} (55.7 Å)). ϵ_S and ϵ_R are dielectric constants of solvents used for photophysical studies and for measuring the redox potentials, respectively. [b] The $k_{CS(P^*-C)}$ and $\Phi_{CS(P^*-C)}$ values were calculated from eqs 11 and 12, respectively. [c] From Figure 7b.

The $\Phi_{EN(P^*-C)}$ values in PhCN and *o*-DCB are summarized in Table 3. For all *n*T's, the $\Phi_{EN(P^*-C)}$ values considerably decreased with an increase in solvent polarity, suggesting that the CS process becomes predominant in polar solvents. In Table 2, the k_q values of $^1H_2P^*$-*n*T in polar solvents are slightly larger than the corresponding k_q values in toluene. This finding implies that the slow CS process occurs from the *n*T moiety to the $^1H_2P^*$, producing $H_2P^{\cdot-}$-*n*T$^{\cdot+}$ because this process has negative ΔG_{CS} values in polar solvents (Supporting Information, Table S2). The $k_{CS(P^*-T)}$ and $\Phi_{CS(P^*-T),dyad}$ values were evaluated by applying eqs 7 and 8 to the τ_F values of $^1H_2P^*$-*n*T; the $k_{CS(P^*-T)}$ and $\Phi_{CS(P^*-T),dyad}$ values in polar solvents are the same as k_q and Φ_q for $^1H_2P^*$-*n*T, as shown in Table 2.

$$k_{CS(P^*-T)} = [\tau_F^{-1}{}_{dyad}(\text{polar solvent}) - \tau_0^{-1}] \quad (7)$$

$$\Phi_{CS(P^*-T),dyad} = \frac{k_{CS(P^*-T),dyad}}{[\tau_F^{-1}{}_{dyad}(\text{polar solvent})]} \quad (8)$$

Because the ΔG_{CS} values for $H_2P^{\cdot-}$-*n*T$^{\cdot+}$ via $^1H_2P^*$-*n*T are similar to those of $H_2P^{\cdot-}$-*n*T$^{\cdot+}$-C_{60} via $^1H_2P^*$-*n*T-C_{60}, we can assume that this type of CS process takes place in the triads at the same rates as in the dyads. The $\Phi_{CS(P^*-T),triad}$ values can be calculated from eq 9, as listed in Supporting Information, Table S3.

$$\Phi_{CS(P^*-T),triad} = \frac{k_{CS(P^*-T),dyad}}{[\tau_F^{-1}{}_{triad}(\text{polar solvent})]} \quad (9)$$

The $\Phi_{CS(P^*-T),triad}$ values are <0.35, which is quite smaller than the corresponding $\Phi_{CS(P^*-T),dyad}$ values in PhCN and *o*-DCB, suggesting that other processes than CS that produce $H_2P^{\cdot-}$-*n*T$^{\cdot+}$ via the $^1H_2P^*$ moiety are present in the triads in polar solvents. The increment of k_q values of the triads in PhCN and *o*-DCB compared with those in toluene can be attributed to the CS process generating $H_2P^{\cdot+}$-*n*T-$C_{60}^{\cdot-}$ via $^1H_2P^*$-*n*T-C_{60}, which is possible because the ΔG_{CS} values are all negative. All of the processes of triads in polar solvents are summarized in eq 10.

$$^1H_2P^*\text{-}n\text{T-}C_{60} \xrightarrow{\substack{k_{q,triad}\,(\text{in polar solvent}) = \\ k_{CS(P^*-C)} + k_{CS(P^*-T)} + k_{EN(P^*-C)}}} H_2P^{\cdot+}\text{-}n\text{T-}C_{60}^{\cdot-} + H_2P^{\cdot-}\text{-}n\text{T}^{\cdot+}\text{-}C_{60} + H_2P\text{-}n\text{T-}^1C_{60}^* \quad (10)$$

The $k_{CS(P^*-C)}$ and $\Phi_{CS(P^*-C)}$ values for this CS process were calculated by subtracting the rate constants due to the previously discussed processes ($k_d + k_{EN(P^*-C)} + k_{CS(P^*-T)}$) from the observed τ_F^{-1} values for $^1H_2P^*$-*n*T-C_{60} in polar solvents as eqs 11 and 12, respectively:

$$k_{CS(P^*-C)} = [\tau_F^{-1}{}_{triad}(\text{polar solvent}) - \{k_d + k_{EN(P^*-C)} + k_{CS(P^*-T)}\}] \quad (11)$$

$$\Phi_{CS(P^*-C)} = \frac{k_{CS(P^*-C)}}{[\tau_F^{-1}{}_{triad}(\text{polar solvent})]} \quad (12)$$

The $k_{CS(P^*-C)}$ and $\Phi_{CS(P^*-C)}$ values are listed in Table 4, in which the $k_{CS(P^*-C)}$ value decreased from 1.7×10^9 to 6.9×10^8 s^{-1} in PhCN and from 8.6×10^8 to 1.3×10^7 s^{-1} in *o*-DCB by changing from 4T to 12T. For $^1H_2P^*$-4T-C_{60} in PhCN and *o*-DCB, the comparison of the $\Phi_{CS(P^*-C)}$ with $\Phi_{EN(P^*-C)}$ values indicates that the main process was EN, whereas CS becomes predominant for the other triads. For H_2P-12T-C_{60}, the CS process becomes predominant in PhCN, whereas in *o*-DCB, both processes become minor. In $^1H_2P^*$-4T-C_{60} and $^1H_2P^*$-8T-C_{60}, the contribution of the CS process generating $H_2P^{\cdot+}$-*n*T-$C_{60}^{\cdot-}$ is larger than that of the CS process generating $H_2P^{\cdot-}$-*n*T$^{\cdot+}$-C_{60}, whereas the contribution of the latter CS process increases when generating $H_2P^{\cdot-}$-12T$^{\cdot+}$-C_{60} in PhCN and *o*-DCB.

Picosecond Transient Absorption Study by Excitation of the H_2P Moiety in PhCN. When the H_2P moiety of H_2P-12T-C_{60} was selectively excited with the 150-fs laser light at 560 nm in PhCN, the absorption spectra were observed as shown in Figure 7a, in which the absorption around 600−650 nm and the broad band around 700−850 nm with a tail to 1100 nm were observed at 100 ps. Compared with the transient spectra of H_2TPP as shown in Supporting Information, Figure S3, it is revealed that the $^1H_2P^*$ moiety has broad absorptions in the visible and near-IR regions.[29f] Thus, the main absorption band around 600−650 nm of H_2P-12T-C_{60} at 100 ps was attributed to the $^1H_2P^*$ moiety. From the initial decay of the 650 nm band of the $^1H_2P^*$ moiety, the rate constant was estimated to be 1.5×10^9 s^{-1}, which is in good agreement with the fluorescence decay rate of $^1H_2P^*$-12T-C_{60} ($\tau_{F(PhCN)}^{-1} = 1.5 \times 10^9$ s^{-1} in PhCN in Table 2). After the decay of the $^1H_2P^*$ moiety, the absorption bands remain around 720 and 1020 nm at 2 ns, which can be attributed to the $H_2P^{\cdot+}$ and $C_{60}^{\cdot-}$ moieties, respectively.[51,52] At 700 nm, the rise of the $H_2P^{\cdot+}$ moiety was indicated as shown in Figure 7b. This finding suggests that the CS state, $H_2P^{\cdot+}$-12T-$C_{60}^{\cdot-}$, was produced via $^1H_2P^*$-12T-C_{60}. Similarly, the following reactions (eq 13) were confirmed for H_2P-4T-C_{60} and H_2P-8T-C_{60}:

$$^1H_2P^*\text{-}n\text{T-}C_{60} \xrightarrow{\substack{k_{CS(P^*-C)} = \\ \Phi_{CS(P^*-C)} \times k_{rise}(H_2P^{\cdot+})}} H_2P^{\cdot+}\text{-}n\text{T-}C_{60}^{\cdot-} \quad (13)$$

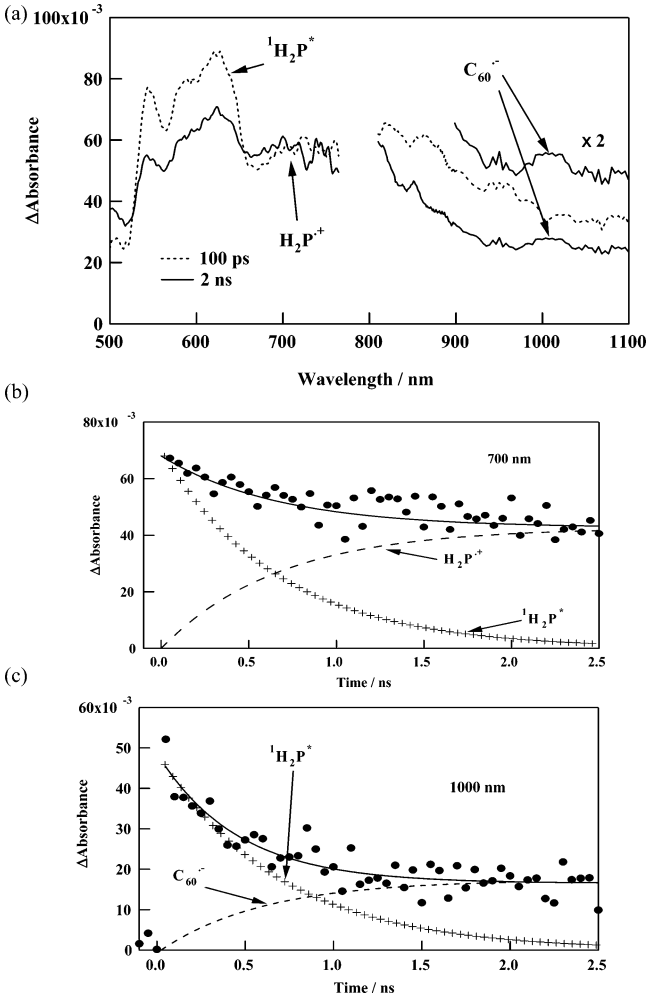

Figure 7. (a) Picosecond transient absorption spectra observed at 100 ps and 2 ns by the 560-nm laser excitation of H_2P-12T-C_{60} (2.0×10^{-4} M) in PhCN. (b and c) Absorption-time profiles around 700 and 1000 nm. The solid curves indicate the best-fit exponential curve (eq 14).

Because the absorption bands of the $H_2P^{\cdot+}$ and $C_{60}^{\cdot-}$ moieties are overlapped with the wide absorption bands of the $^1H_2P^*$ moiety in the 700−1100-nm regions, these temporal profiles can be analyzed on the basis of eq 14.

$$\Delta\mathrm{Abs} = \mathrm{A}_1\{\exp(-k_{\mathrm{decay}})\} + \mathrm{A}_2\{1 - \exp(-k_{\mathrm{rise}})\} \quad (14)$$

The temporal profiles (solid curve) can be fitted by setting the k_{decay} and k_{rise} values equal to $1/\tau_{\mathrm{F(PhCN)}}$. As shown in Figure 7b (at 700 nm) and Figure 7c (at 1000 nm), the temporal profile is well fitted after assigning 1.5×10^9 s^{-1} from Table 2 to k_{decay} and k_{rise} in the case of H_2P-12T-C_{60}. Taking the $\Phi_{\mathrm{CS(P^*-C)}}$ (0.47 from Table 4) into consideration, we calculated the rate constant ($k_{\mathrm{CS(P^*-C)}}$) to be 7.0×10^8 s^{-1} for the generation of the $H_2P^{\cdot+}$ moiety from the $^1H_2P^*$ moiety. Because the absorption band attributed to the $C_{60}^{\cdot-}$ moiety was overlapped with the absorption of the $^1H_2P^*$ moiety, the curve-fitting was performed as shown in Figure 7c, in which the rise component of the $C_{60}^{\cdot-}$ moiety was confirmed to have the same rate constant as the decay of the $^1H_2P^*$ moiety. This finding supports the direct generation of $H_2P^{\cdot+}$-12T-$C_{60}^{\cdot-}$ from $^1H_2P^*$-12T-C_{60}. In the cases of H_2P-4T-C_{60} and H_2P-8T-C_{60}, the generation of the $H_2P^{\cdot+}$ moiety was also confirmed by a 720-nm band. The $k_{\mathrm{CS(P^*-C)}}$ value for $H_2P^{\cdot+}$-8T-$C_{60}^{\cdot-}$ was calculated to be 1.4×10^9 s^{-1}, which is in good agreement with the $k_{\mathrm{CS(P^*-C)}}$ value calculated from the time-resolved fluorescence measurement. In the case of H_2P-4T-C_{60}, the curve fittings to the decay of the $^1H_2P^*$ moiety and the rise of the $H_2P^{\cdot+}$ moiety were similarly possible, although the analysis of the 1000-nm region was difficult because the rise of $C_{60}^{\cdot-}$ may include the CS process via $^1C_{60}^*$ after EN from $^1H_2P^*$ in addition to the direct CS process (eq 13).

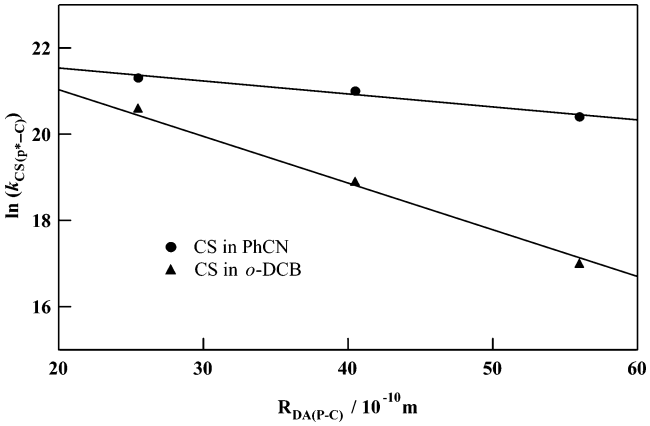

Figure 8. Donor−acceptor distance ($R_{\mathrm{DA(P-C)}}$) dependence of the CR rate constants. Plots of ln($k_{\mathrm{CS(P^*-C)}}$) vs $R_{\mathrm{DA(P-C)}}$ in PhCN (●) and *o*-DCB (▲) for H_2P-*n*T-C_{60}. The lines represent the best fit to eq 15.

In *o*-DCB, the picosecond transient absorption measurement failed to work because the H_2P moiety was degraded seriously by the intense femtosecond laser in solvents including halogen atoms.

Function of *n*T as a Molecular Wire. From Figure 7, because the transient absorption bands of $^1H_2P^*$, $H_2P^{\cdot+}$, and $C_{60}^{\cdot-}$ were independently confirmed, the direct formation of $H_2P^{\cdot+}$-*n*T-$C_{60}^{\cdot-}$ via $^1H_2P^*$-*n*T-C_{60} was revealed. Hence, it is possible to calculate an attenuation factor for the oligothiophenes. Figure 8 shows the plots of ln($k_{\mathrm{CS(P^*-C)}}$) versus $R_{\mathrm{DA(P-C)}}$ for H_2P-*n*T-C_{60} in PhCN and *o*-DCB, where the $R_{\mathrm{DA(P-C)}}$ values are 25.5, 40.4, and 55.7 Å for H_2P-4T-C_{60}, H_2P-8T-C_{60}, and H_2P-12T-C_{60}, respectively (Figure 2). The plots show a linear relationship between ln($k_{\mathrm{CS(P^*-C)}}$) and $R_{\mathrm{DA(P-C)}}$ with negative slopes, which indicate that the $k_{\mathrm{CS(P^*-C)}}$ values become smaller with the increasing length of *n*T. This finding indicates that the *n*T moiety acts as a molecular wire for the direct CS process in eq 13. In general, the distance dependence of the CS rate constants (k_{CS}) is described by eq 15,[43,53−56]

$$\ln(k_{\mathrm{CS}}) = \ln\left[\frac{2\pi^{3/2}V_0^{\,2}}{h(\lambda k_{\mathrm{B}}T)^{1/2}}\right] - \beta R_{\mathrm{DA}} \quad (15)$$

where V_0 refers to a maximal electronic coupling and β refers to a damping factor that depends primarily on the nature of the bridge molecule. The β values for $k_{\mathrm{CS(P^*-C)}}$ of H_2P-*n*T-C_{60} were estimated to be 0.03 $Å^{-1}$ in PhCN and 0.11 $Å^{-1}$ in *o*-DCB using eq 15. An appreciable solvent polarity effect was found in the β values for $k_{\mathrm{CS(P^*-C)}}$; that is, the CS process from the $^1H_2P^*$ moiety to the C_{60} moiety in polar PhCN takes place through longer *n*T moieties than that in less polar *o*-DCB, which implies that the ability of the molecular wire of the *n*T moieties is promoted by the surrounding polar solvents.

These β values are much smaller than the reported β values for saturated hydrocarbon bridges (0.6−1.2 $Å^{-1}$)[53] and conjugated *p*-phenylenes (0.32−0.66 $Å^{-1}$),[54] whereas the β values for H_2P-*n*T-C_{60} are comparable to those for oligoenes (0.04−0.2 $Å^{-1}$)[55] and oligoynes (0.04−0.17 $Å^{-1}$).[56] These small β values indicate that the *n*T moieties serve as

TABLE 5: Free Energy Changes (ΔG_{CR})[a] and Rate Constants ($k_{CR(T-C)}$) for Charge Recombination (CR) and Lifetimes of the Radical Ion Pair (τ_{RIP}) in PhCN and *o*-DCB Observed by Transient Absorption Measurements

				$n = 4$			$n = 8$			$n = 12$		
solvent	initial state	final state	k_{CR}	$-\Delta G_{CR}$ (eV)	k_{CR} (s^{-1})	τ_{RIP} (μs)	$-\Delta G_{CR}$ (eV)	k_{CR} (s^{-1})	τ_{RIP} (μs)	$-\Delta G_{CR}$ (eV)	k_{CR} (s^{-1})	τ_{RIP} (μs)
PhCN	H_2P-*n*T$^{\cdot+}$-$C_{60}^{\cdot-}$	H_2P-*n*T-C_{60}	($k_{CR(T-C)}$)[b]	1.40	4.2×10^5 [b]	2.4	1.32	5.2×10^5 [b]	1.9	1.25	6.9×10^5 [b]	15
o-DCB	H_2P-*n*T$^{\cdot+}$-$C_{60}^{\cdot-}$	H_2P-*n*T-C_{60}	($k_{CR(T-C)}$)[b]	1.52	7.1×10^4	14	1.42	3.7×10^4	27	1.35	5.1×10^4	20

[a] The ΔG_{CR} values were calculated from eqs 1 and 2; see the margin of Table 4. [b] The $k_{CR(T-C)}$ values were estimated from the absorption decay time profile of H_2P-*n*T$^{\cdot+}$-$C_{60}^{\cdot-}$ in the transient measurements in nanosecond−microsecond regions.

superior molecular wires allowing an efficient long-range CS process from the $^1H_2P^*$ moiety to the C_{60} moiety through the *n*T moiety.

Hole Shift and the Charge-Recombination Process. Figure 9 shows the nanosecond transient absorption spectra of H_2P-12T-C_{60} observed with 560-nm pulse (fwhm 4 ns) irradiation, which predominantly excites the H_2P moiety. In the spectrum at 250 ns, the transient absorption bands of the 12T$^{\cdot+}$ moiety appeared in the region of 840 nm and >1300 nm, and those of the $C_{60}^{\cdot-}$ moiety appeared at 1000 nm, in addition to the absorption bands of the $^3H_2P^*$ and $^3C_{60}^*$ moieties in the region of 700−800 nm in PhCN.[28,57] From the ratio of the absorption intensity of the 12T$^{\cdot+}$ moiety to that of $C_{60}^{\cdot-}$,[28] the generation of H_2P-12T$^{\cdot+}$-$C_{60}^{\cdot-}$ was confirmed by the spectrum at 250 ns after the photoexcitation. This finding indicates that H_2P-12T$^{\cdot+}$-$C_{60}^{\cdot-}$ was generated via $H_2P^{\cdot+}$-12T-$C_{60}^{\cdot-}$; therefore, the hole of the $H_2P^{\cdot+}$ moiety shifted to the 12T moiety after the nanosecond laser pulse. Similar transient absorption spectra were observed by the selective excitation of the H_2P moiety of H_2P-4T-C_{60} and H_2P-8T-C_{60}. From the comparison of the absorption intensity of the 4T$^{\cdot+}$ moiety (700 and 1140 nm)[28,57] and the 8T$^{\cdot+}$ moiety (850 and >1300 nm)[28,57] with that of the $C_{60}^{\cdot-}$ moiety, the formations of H_2P-4T$^{\cdot+}$-$C_{60}^{\cdot-}$ and H_2P-8T$^{\cdot+}$-$C_{60}^{\cdot-}$ are also confirmed by the spectra of the microsecond region.

Figure 8b shows the absorption-time profile at 1520 nm of the 12T$^{\cdot+}$ moiety, which indicates the hole shift from $H_2P^{\cdot+}$-12T-$C_{60}^{\cdot-}$ to H_2P-12T$^{\cdot+}$-$C_{60}^{\cdot-}$ as shown in eq 16 at 50 ns. From this rise, the rate constant for this hole-shift process ($k_{HS((P-T)}$ in eq 16) was estimated to be 7.0×10^7 s^{-1} for H_2P-12T-C_{60}. Similar $k_{HS(P-T)}$ values were calculated for H_2P-4T-C_{60} and H_2P-8T-C_{60} as listed in Table 4. An appreciable solvent polarity effect was not found in the $k_{HS(P-T)}$ values.

$$H_2P^{\cdot+}\text{-}n\text{T-}C_{60}^{\cdot-} \xrightarrow{\text{hole shift, } k_{HS(P-T)}} H_2P\text{-}n\text{T}^{\cdot+}\text{-}C_{60}^{\cdot-} \quad (16)$$

From the microsecond-region decay profiles shown in Figure 9c and d, which consist of the single-exponential decay, the rate constant for the decay of H_2P-12T$^{\cdot+}$-$C_{60}^{\cdot-}$ was calculated. Becuase the *n*T$^{\cdot+}$ moiety and the $C_{60}^{\cdot-}$ moiety decayed at the same rate, this process can be attributed to the CR process of H_2P-12T$^{\cdot+}$-$C_{60}^{\cdot-}$ (eq 17). For all triads, the $k_{CR(T-C)}$ values were calculated to be on the order of 10^5 s^{-1} in PhCN as listed in Table 5. In *o*-DCB, the nanosecond transient spectra were possible to measure because the intensity of the 4-ns laser was much lower than that of the 150-fs laser; the $k_{CR(T-C)}$ values were similarly calculated to be on the order of 10^4 s^{-1} for all triads, as listed in Table 5. Note that the $k_{CR(T-C)}$ values are quite small in *o*-DCB, indicating that the lifetimes (τ_{RIP}) of H_2P-*n*T$^{\cdot+}$-$C_{60}^{\cdot-}$ in less polar solvents are longer than 10 μs. It has been reported that both *n*T$^{\cdot+}$ and $C_{60}^{\cdot-}$ are not reactive to O_2;[58] however, both decay rates of the 12T$^{\cdot+}$ and $C_{60}^{\cdot-}$ moieties in H_2P-12T$^{\cdot+}$-$C_{60}^{\cdot-}$ were accelerated in the presence of O_2, as shown in Figure 9c. Similar phenomena were

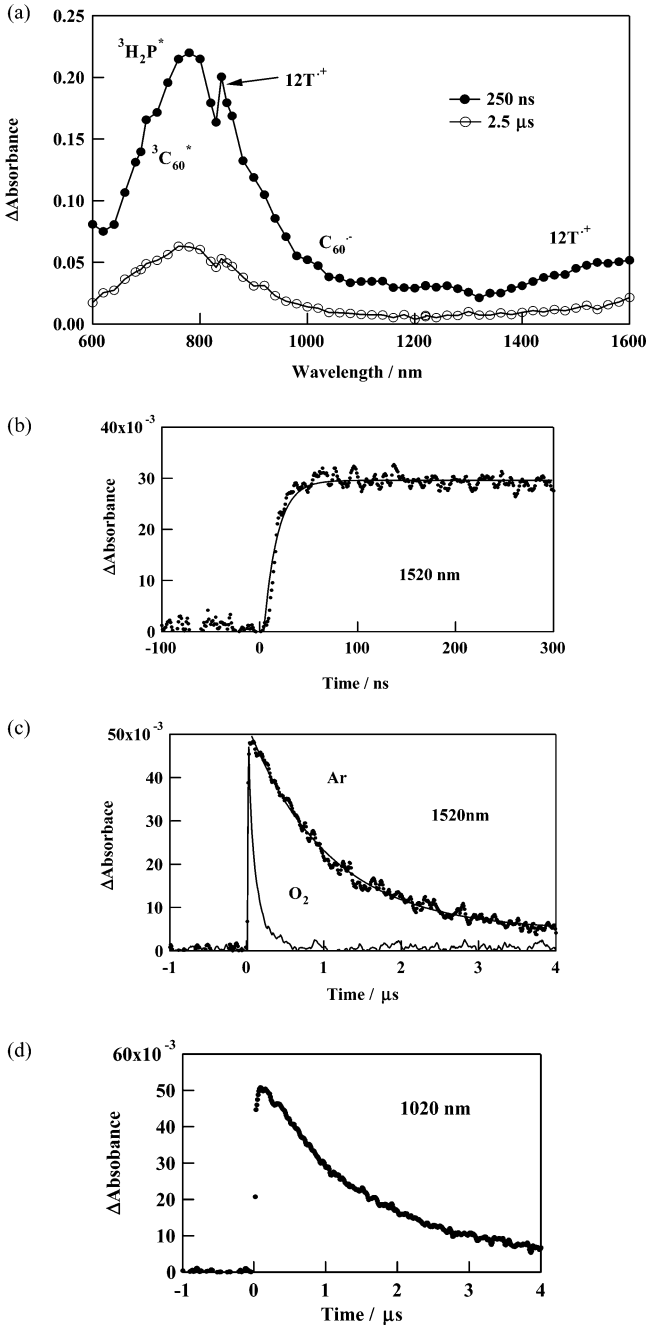

Figure 9. (a) Nanosecond transient absorption spectra observed at 250 ns (●) and 2.5 μs (○) after 560-nm laser light excitation of H_2P-12T-C_{60} (1.0×10^{-4} M) in Ar-saturated PhCN. (b and c) Absorption-time profile at 1520 nm. (d) Absorption-time profile at 1020 nm.

observed for other H_2P-*n*T$^{\cdot+}$-$C_{60}^{\cdot-}$. This finding indicates that H_2P-*n*T$^{\cdot+}$-$C_{60}^{\cdot-}$ gains triplet character by mixing with the triplet states of H_2P-*n*T-C_{60}, which have a similar energy to that of

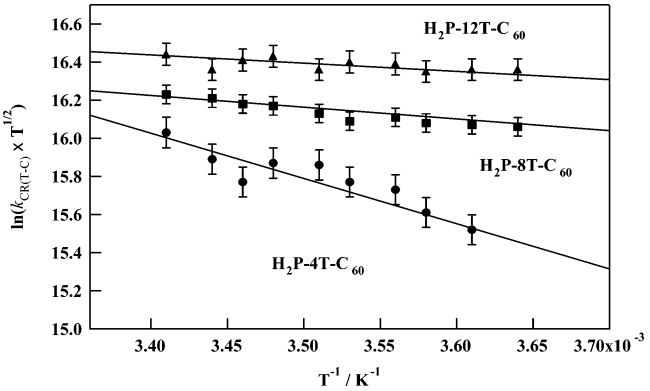

Figure 10. Modified Arrhenius plots (eq 18) of the temperature-dependent $k_{CR(T-C)}$ for H_2P-4T-C_{60} (●), H_2P-8T-C_{60} (■), and H_2P-12T-C_{60} (▲).

H_2P-nT$^{\cdot+}$-$C_{60}^{\cdot-}$. This is one of the interpretations for such long τ_{RIP} values of H_2P-nT$^{\cdot+}$-$C_{60}^{\cdot-}$.

$$H_2P\text{-}n\text{T}^{\cdot+}\text{-}C_{60}^{\cdot-} \xrightarrow{k_{CR(T-C)}} H_2P\text{-}n\text{T-}C_{60} \qquad (17)$$

To estimate experimentally the energy barrier for the CR step from H_2P-nT$^{\cdot+}$-$C_{60}^{\cdot-}$ to H_2P-nT-C_{60}, we measured the $k_{CR(T-C)}$ values of H_2P-nT$^{\cdot+}$-$C_{60}^{\cdot-}$ as a function of the temperature in PhCN (275−293 K) and *o*-DCB (265−298 K). The $k_{CR(T-C)}$ values of H_2P-nT$^{\cdot+}$-$C_{60}^{\cdot-}$ increased with an increase in the temperature; that is, the $k_{CR(T-C)}$ values in H_2P-4T$^{\cdot+}$-$C_{60}^{\cdot-}$ changed from 5.0×10^5 to 9.2×10^5 s^{-1} in PhCN and from 4.9×10^4 to 6.2×10^4 s^{-1} in *o*-DCB. Such differences in the $k_{CR(T-C)}$ values are larger than the experimental error in our measurements. In general, the CR rate constant ($k_{CR(T-C)}$) can be described by the semiclassical Marcus equation (eq 18);[43]

$$\ln(k_{CR(T-C)}T^{1/2}) = \ln\left[\frac{2\pi^{3/2}V^2}{h(\lambda k_B)^{1/2}}\right] + \left(\frac{-\Delta G_{CR}^{\ddagger}}{k_B T}\right) \qquad (18)$$

Hereby T, h, k_B, and $\Delta G_{CR}^{\ddagger}$ refer to temperature, Planck's constant, the Boltzman constant, and the Gibbs activation energy in Marcus theory, respectively.[43] The λ and V are referred to as the reorganization energy and electron-coupling matrix element for the CR process, respectively.

The plots of the observed $\ln(k_{CR(T-C)}T^{1/2})$ values versus $1/T$ gave the linear relations as shown in Figure 10. From the slope that is equal to $-\Delta G_{CR(T-C)}^{\ddagger}/k_B$, the values of $\Delta G_{CR(T-C)}^{\ddagger}$ in PhCN were determined to be 0.20, 0.05, and 0.04 eV for H_2P-nT$^{\cdot+}$-$C_{60}^{\cdot-}$ (n = 4, 8, and 12, respectively); in *o*-DCB, the corresponding $\Delta G_{CR(T-C)}^{\ddagger}$ values were estimated to be 0.11, 0.02, and 0.01 eV. The $\Delta G_{CR(T-C)}^{\ddagger}$ values decrease drastically from 4T to 8T. The $\Delta G_{CR(T-C)}^{\ddagger}$ values in polar PhCN are larger than the corresponding values in less polar *o*-DCB.

The λ values for the CR process were evaluated using eq 19[43] by setting $\Delta G_0 = \Delta G_{CR(T-C)}$, in which the latter values are listed in Table 5.

$$\Delta G_{CR(T-C)}^{\ddagger} = \frac{(\Delta G_0 + \lambda)^2}{4\lambda} \qquad (19)$$

The calculated λ values in PhCN (0.80, 0.94, and 0.89 eV for H_2P-nT$^{\cdot+}$-$C_{60}^{\cdot-}$ (n = 4, 8, and 12, respectively)) are slightly smaller than the corresponding ones in *o*-DCB (0.90, 1.20, and 1.10 eV). The λ values are in the order of 4T < 12T ≤ 8T, which suggests that the charge density of H_2P-4T$^{\cdot+}$-$C_{60}^{\cdot-}$ is much larger than those in the other triads, whereas the difference in the charge densities between 8T and 12T is small[59] because the reorganization energy due to the solvation factor generally tends to decrease with the larger charged surface area.[43] This implies that the hole along the π conjugation in 8T and 12T tends to localize in the middle part of the chain more than that in 4T because the charge per thiophene ring takes a maximum point in the middle of the chain for 8T and 12T.[59] A slight increase in the λ values was observed in *o*-DCB compared to the corresponding values in PhCN, indicating that the interaction between the solvents and charged solute also affects the λ values.[43]

Because the λ values are smaller than the absolute values of $\Delta G_{CR(T-C)}$, the CR processes of H_2P-nT$^{\cdot+}$-$C_{60}^{\cdot-}$ occur in the Marcus inverted region. As shown in Table 5, H_2P-4T$^{\cdot+}$-$C_{60}^{\cdot-}$ has the longest lifetime in PhCN, which is due to the smallest λ value and largest $|\Delta G_{CR(T-C)}|$. These factors predict a smaller $k_{CR(T-C)}$ value for H_2P-4T-C_{60} than for H_2P-8T-C_{60} and H_2P-12T-C_{60}. A similar trend was observed in *o*-DCB.

The V values for the CR process in PhCN were calculated to be 1.20, 0.14, and 0.11 cm^{-1} for H_2P-nT$^{\cdot+}$-$C_{60}^{\cdot-}$ (n = 4, 8, and 12, respectively) from the intercept of Figure 10 (the first term of eq 18). The V values for H_2P-8T$^{\cdot+}$-$C_{60}^{\cdot-}$ and H_2P-12T$^{\cdot+}$-$C_{60}^{\cdot-}$ are extremely small compared to the reported V values (1−100 cm^{-1}) for conventional dyad systems.[18,19] Such extremely small V values are the origin of small $k_{CR(T-C)}$ values. The extremely large V value of H_2P-4T$^{\cdot+}$-$C_{60}^{\cdot-}$ compared to those of H_2P-8T$^{\cdot+}$-$C_{60}^{\cdot-}$ and H_2P-12T$^{\cdot+}$-$C_{60}^{\cdot-}$ is also due to the charge density of the nT$^{\cdot+}$ moiety. In *o*-DCB, smaller V values (0.14, 0.02, and 0.02 cm^{-1} for H_2P-nT$^{\cdot+}$-$C_{60}^{\cdot-}$ (n = 4, 8, and 12, respectively)) were calculated, supporting smaller $k_{CR(T-C)}$ values.

Conclusions

In polar solvents, the initial CS states were revealed to be $H_2P^{\cdot+}$-nT-$C_{60}^{\cdot-}$ produced via ^1H_2P*-nT-C_{60}, in which the nT moieties act as efficient molecular wires. The ability of molecular wires strongly depends on the solvent polarity; the β value for this CS process was as small as 0.03 Å^{-1} in PhCN; therefore, the nT's are superior molecular wires. Then, the hole shift takes place from $H_2P^{\cdot+}$-nT-$C_{60}^{\cdot-}$ to H_2P-nT$^{\cdot+}$-$C_{60}^{\cdot-}$; in this process, the nT's act as hole acceptors. Finally, the CR takes place in H_2P-nT$^{\cdot+}$-$C_{60}^{\cdot-}$, in which the nT$^{\cdot+}$ moiety acts as an electron acceptor from the $C_{60}^{\cdot-}$ moiety. The lifetimes of H_2P-nT$^{\cdot+}$-$C_{60}^{\cdot-}$ were longer than 10 μs in *o*-DCB. In nonpolar solvents, the EN process is competitive with the CS process. In the EN process, the nT's act as spacers. The lengths and the free-energy changes of the nT's governed the precedence of the paths. Thus, multifunctional roles of the nT's in the photoinduced processes of H_2P-nT-C_{60} were revealed in the present study.

Acknowledgment. The present work was partially supported by a Grant-in-Aid for Scientific Research on Primary Area (417) from the Ministry of Education, Science, Sports, and Culture of Japan and (nos. 10207202, 11740380, and 12875163). We are also grateful to the Mitsubishi foundation.

Supporting Information Available: Optimized structures in different solvents, free-energy changes, and driving forces for charge separation, charge recombination, and hole transfer. Rate constants and quantum yields. Calculation of energy-transfer rate constants and picosecond transient spectra of reference compounds. This material is available free of charge via the Internet at http://pubs.acs.org.

References and Notes

(1) (a) Mitschke, U.; Bäuerle, P. *J. Mater. Chem.* **2000**, *10*, 1471. (b) Shirota, Y. *J. Mater. Chem.* **2000**, *10*, 1.

(2) (a) Harrison, M. G.; Friend R. H. In *Electronic Materials: The Oligomer Approach*; Müllen, K., Wegner, G., Eds.; Wiley-VCH: Weinheim, Germany, 1998; pp 515−558. (b) van Duren, J. K. J.; Dhanabalan, A.; van Hal, P. A.; Janssen, R. A. J. *Synth. Met.* **2001**, *121*, 1587. (c) Brabec, C. J.; Shaheen, S. E.; Fromherz, T.; Padinger, F.; Hummelen, J. C.; Dhanabalan, A.; Janssen, R. A. J.; Sariciftci, N. S. *Synth. Met.* **2001**, *121*, 1517. (d) Winder, C.; Matt, G.; Hummelen, J. C.; Janssen, R. A. J.; Sariciftci, N. S.; Brabec, C. J. *Thin Solid Films* **2002**, *403*−*404*, 373.

(3) (a) Horowitz, G. *Adv. Mater*. **1998**, *10*, 365. (b) Dimitrakopoulos, C. D.; Malenfant, P. R. M. *Adv. Mater.* **2002**, *14*, 99.

(4) Nalwa, H. S., Ed. *Handbook of Organic Conductive Molecules and Polymers*, Vol. 4; John Wiley: Chichester, U.K., 1997; pp 261−363.

(5) (a) Nakanishi, H.; Sumi, N.; Aso, Y.; Otsubo, T. *J. Org. Chem.* **1988**, *53*, 8632. (b) Nakanishi, H.; Aso, Y.; Otsubo, T. *Synth. Met.* **1999**, *101*, 413. (c) Nakanishi, H.; Sumi, N.; Ueno, S.; Takimiya, K.; Aso, Y.; Otsubo, T.; Komaguchi, K.; Shiotani, M.; Ohta, N. *Synth. Met*. **2001**, *119*, 413.

(6) (a) Otsubo, T.; Aso, Y.; Takimiya, K. *Bull. Chem. Soc. Jpn.* **2001**, *74*, 1789. (b) Otsubo, T.; Aso, Y.; Takimiya, K. *J. Mater. Chem.* **2002**, *12*, 2565.

(7) (a) Roncali, J. *Chem. Rev.* **1992**, *92*, 711. (b) Becker, R. S.; de Melo, J. S.; Maçanita, A. L.; Elisei, F. *Pure Appl. Chem.* **1995**, *67*, 9. (c) Smith, J. R.; Cox, P. A.; Campbell, S. A.; Ratcliffe, N. M. *J. Chem. Soc., Faraday Trans.* **1995**, *91*, 2331. (d) Apperloo, J. J.; Janssen, R. A. J.; Malenfant, P. R. L.; Fréchet, J. M. J. *J. Am. Chem. Soc.* **2001**, *123*, 6919. (e) Greve, D. R.; Apperloo, J. J.; Janssen, R. A. J. *Synth. Met.* **2001**, *119*, 369. (f) Apperloo, J. J.; Malenfant, P. R. L.; Fréchet, J. M. J.; Janssen, R. A. J. *Synth. Met.* **2001**, *121*, 1259. (g) Vonk, E. C.; Langeveld-Voss, B. M. W.; Van Dongen, J. L. J.; Janssen, R. A. J.; Claessens, H. A.; Cramers, C. A. *J. Chromatogr., A* **2001**, *911*, 13. (h) Jiang, X. M.; Österbacka, R.; Korovyanko, O.; An, C. P.; Horovitz, B.; Janssen, R. A. J.; Vardeny, Z. V. *Adv. Funct. Mater.* **2002**, *12*, 709. (i) van Hal, P. A.; Janssen, R. A.; Lanzani, G.; Cerullo, G.; Zavelani-Rossi, M.; De Silvestri, S. *Chem. Phys. Lett.* **2001**, *345*, 33.

(8) (a) Segawa. H.; Wu, F.-P.; Nakayama, N.; Maruyama, H.; Sagisaka, S.; Higuchi, N.; Fujitsuka, M.; Shimidzu, T. *Synth. Met.* **1995**, *71*, 2151. (b) Fujitsuka, M.; Sato, T.; Segawa, H.; Simidzu, T. *Synth. Met.* **1995**, *69*, 309.

(9) Winkler, J. R.; Gray, H. B. *Chem. Rev.* **1992**, *92*, 369.

(10) Langen, R.; Chang, I. J.; Germanas, J. P.; Richards, J. H.; Winkler, J. R.; Gray, H. B. *Science* **1995**, *268*, 1733.

(11) Page, C. C.; Moser, C. C.; Chen, X.; Dutton, P. L. *Nature* **1999**, *402*, 47.

(12) Wasielewski, M. R. *Chem. Rev.* **1992**, *92*, 395.

(13) Verhoeven, J. W.; Scherer, T.; Willemse, R. J. *Pure Appl. Chem*. **1993**, *65*, 1717.

(14) Verhoeven, J. W. *Pure Appl. Chem*. **1990**, *62*, 1585.

(15) Imahori, H.; Sakata, Y. *Eur. J. Org. Chem*. **1999**, 2445.

(16) Imahori, H.; Sakata Y. *Adv. Mater*. **1997**, *9*, 537.

(17) Fukuzumi, S. *J. Phys. Org. Chem.* **2002**, *15*, 448.

(18) (a) Luo, C.; Guldi, D. M.; Imahori, H.; Tamaki, K.; Sakata, Y. *J. Am. Chem. Soc*. **2000**, *122*, 6535. (b) Fukuzumi, S.; Imahori, H.; Yamada, H.; El-Khouly, M. E.; Fujitsuka, M.; Ito, O.; Guldi, D. M. *J. Am. Chem. Soc*. **2001**, *123*, 2571. (c) Imahori, H.; Tamaki, K.; Guldi, D. M.; Luo. C.; Fujitsuka, M.; Ito, O.; Fukuzumi, S. *J. Am. Chem. Soc*. **2001**, *123*, 2607. (d) Imahori, H.; Guldi, D. M.; Tamaki, K.; Yoshida, Y.; Luo, C.; Sakata, Y.; Fukuzumi, S. *J. Am. Chem. Soc*. **2001**, *123*, 6617. (e) Imahori, H.; Tamaki, K.; Araki, Y.; Sekiguchi, Y.; Ito, O.; Sakata, Y.; Fukuzumi, S. *J. Am. Chem. Soc*. **2002**, *124*, 5165.

(19) (a) Lindell, P. A.; Kuciauskas, D.; Sumida, J. P.; Nash, B.; Nguyen, D.; Moore, A. L.; Moore, T. A.; Gust, D. *J. Am. Chem. Soc.* **1997**, *119*, 1400. (b) Carbonera, D.; Di Valentin, M.; Corvaja, C.; Agostini, G.; Giacometti, G.; Liddell, P. A.; Kuciauskas, D.; Moore, A. L.; Moore, T. A.; Gust, D. *J. Am. Chem. Soc.* **1998**, *120*, 4398.

(20) Kroto, H. W.; Heath, J. R.; O'Brien, S, C.; Curl, R. F.; Smalley, R. E. *Nature* **1985**, *318*, 162.

(21) (a) Haddon, R. C. *Acc. Chem. Res.* **1988**, *21*, 243. (b) Haddon, R. C. *Science* **1993**, *261*, 1545.

(22) (a) Maggini, M.; Scorrano, G.; Prato, M. *J. Am. Chem. Soc.* **1993**, *115*, 9798. (b) Guldi, D. M.; Prato, M. *Acc. Chem. Res.* **2000**, *33*, 695.

(23) (a) Allemand, P. H.; Koch, A.; Wudl, F.; Rubin, Y.; Diederich, F.; Alvarenz, M. M.; Anz, S. J.; Whetten, R. L. *J. Am. Chem. Soc.* **1991**, *113*, 1050. (b) Dubois, D.; Kadish, K. M.; Flanagan, S.; Haufler, R. E.; Chibante, L. P. F.; Wilson, L. J. *J. Am. Chem. Soc*. **1991**, *113*, 4364.

(24) Guldi, D. M.; Asmus, K.-D. *J. Am. Chem. Soc.* **1997**, *119*, 5744.

(25) (a) Williams, R. M.; Zwier, M. N.; Verhoeven, J. W. *J. Am. Chem. Soc.* **1995**, *117*, 4093. (b) Williams, R. M.; Koeberg, M.; Lawson, J. M.; An, Y.-Z.; Rubin, Y.; Paddon-Row, M. N.; Verhoeven, J. W. *J. Org. Chem.* **1996**, *61*, 5055. (c) Komamine, S.; Fujitsuka, M.; Ito, O.; Moriwaki, K.; Miyata, T.; Ohno, T. *J. Phys. Chem. A* **2000**, *104*, 11497.

(26) Imahori, H.; Cardoso, S.; Tatman, D.; Lin, S.; Noss, L.; Seely, G. R.; Sereno, L.; Silber, C.; Moore, T. A.; Moore, A. L.; Gust, D. *Photochem. Photobiol.* **1995**, *62*, 1009.

(27) (a) Guldi, D. M.; Maggini, M.; Scorrano, G.; Prato, M. *J. Am. Chem. Soc.* **1997**, *119*, 974. (b) D'Souza, F.; Zandeler, M.; Smith, P. M.; Deviprasad, G. R.; Arkady, K.; Fujitsuka, M.; Ito, O. *J. Phys. Chem. A* **2002**, *106*, 649. (c) Fujitsuka, M.; Tsuboya, N.; Hamasaki, R.; Onodera, S.; Ito, O.; Yamamoto, Y. *J. Phys. Chem. A* **2003**, *107*, 1452.

(28) (a) Fujitsuka, M.; Ito, O.; Yamashiro, T.; Aso, Y.; Otsubo, T. *J. Phys. Chem. A* **2000**, *104*, 4876. (b) Fujitsuka, M.; Matsumoto, K.; Ito, O.; Yamashiro, T.; Aso, Y.; Otsubo, T. *Res. Chem. Intermed.* **2001**, *27*, 73. (c) Fujitsuka, M.; Masuhara, A.; Kasai, H.; Oikawa, H.; Nakanishi, H.; Ito, O.; Yamashiro, T.; Aso, Y.; Otsubo, T. *J. Phys. Chem. B* **2001**, *105*, 9930. (d) Hirayama, D.; Takimiya, K.; Aso, Y.; Otsubo, T.; Hasobe, T.; Yamada, H.; Imahori, H.; Fukuzumi, S.; Sakata, Y. *J. Am. Chem. Soc.* **2002**, *124*, 532. (e) van Hal, P. A.; Beckers, E. H. A.; Meskers, S. C. J.; Janssen, R. A. J.; Jousselme, B.; Blanchard, P.; Roncali, J. *Chem.—Eur. J.* **2002**, *8*, 5415.

(29) (a) Imahori, H.; Hagiwara, K.; Akiyama, T.; Aoki, M.; Taniguchi, S.; Okada, T.; Shirakawa, M.; Sakata, Y. *Chem. Phys. Lett.* **1996**, *263*, 545. (b) Imahori, H.; Hagiwara, K.; Aoki, M.; Akiyama, T.; Taniguchi, S.; Okada, T.; Shirakawa, M.; Sakata, Y. *J. Am. Chem. Soc.* **1996**, *118*, 11771. (c) Imahori, H.; Ozawa, S.; Uchida, K.; Takahashi, M.; Azuma, T.; Ajavakom, A.; Akiyama, T.; Hasegawa, M.; Taniguchi, S.; Okada, T.; Sakata, Y. *Bull. Chem. Soc. Jpn.* **1999**, *72*, 485. (d) Fukuzumi, S.; Ohkubo, K.; Imahori, H.; Shao, J.; Ou. Z.; Zheng, G.; Chen, Y.; Pandey, K. R.; Fujitsuka, M.; Ito, O.; Kadish, K. *J. Am. Chem. Soc.* **2001**, *123*, 10676. (e) Fukuzumi, S.; Imahori, H.; Okamoto, K.; Yamada, H.; Fujitsuka, M.; Ito, O.; Guldi, D. M. *J. Phys. Chem. A* **2002**, *106*, 1903. (f) Imahori, H.; El-Khouly, M. E.; Fujitsuka, M.; Ito, O.; Sakata, Y.; Fukuzumi, S. *J. Phys. Chem. A* **2001**, *105*, 325.

(30) (a) Liddell, P. A.; Sumida, J. P.; Macpherson, A, N.; Noss, L.; Seely, G. R.; Clark, K. N.; Moore, A. L.; Moore, T. A.; Gust, D. *Photochem. Photobiol.* **1994**, *60*, 537. (b) Kuciauskas, D.; Lin, S.; Seely, G. R.; Moore A. L.; Moore, T. A.; Gust, D.; Drovetskaya, T.; Reed, C. A.; Boyd, P. D. W. *J. Phys. Chem.* **1996**, *100*, 15926. (c) Gust, D.; Moore, T. A.; Moore, A. L. *Res. Chem. Intermed.* **1997**, *23*, 621.

(31) (a) Tkachenko, N. V.; Rantala, L.; Tauber, A. Y.; Helaja, J.; Hynninen, P. V.; Lemmetyinen, H. *J. Am. Chem. Soc.* **1999**, *121*, 9378. (b) D'Souza, F.; Deviprasad, G. R.; El-Khouly, M. E.; Fujitsuka, M.; Ito, O. *J. Am. Chem. Soc.* **2001**, *123*, 5277.

(32) Schuster, D. I.; Cheng, P.; Wilson, S. R.; Prokhorenko, V.; Katterle, M.; Holzwarth, A. R.; Braslavsky, S. E.; Klihm, G.; Williams, R. M.; Luo, C. *J. Am. Chem. Soc.* **1999**, *121*, 11599.

(33) Bell, T. D. M.; Smith, T. A.; Ghiggino, K. P.; Ranasinghe, M. G.; Shephard, M. J.; Paddon-Row, M. N. *Chem. Phys. Lett.* **1997**, *268*, 223.

(34) Guldi, D. M.; Garscia, G. T.; Mattay, J. *J. Phys. Chem. A* **1998**, *102*, 9679.

(35) Yamazaki, M.; Araki, Y.; Fujitsuka, M.; Ito, O. *J Phys. Chem. A* **2001**, *105*, 8615.

(36) Martín, N.; Sanchez, L.; Herranz, M. A.; Guldi, D. M. *J. Phys. Chem. A* **2000**, *104*, 4648.

(37) Sariciftci, N. S.; Wudl, F.; Heeger, A. J.; Maggini, M.; Scorrano, G.; Prato, M.; Bourassa, J.; Ford, P. C. *Chem. Phys. Lett.* **1995**, *247*, 510.

(38) Maggini, M.; Guldi, D. M.; Mondini, S.; Scorrano, G.; Paolucci, F.; Ceroni, P.; Roffia, S. *Chem.—Eur. J.* **1998**, *4*, 1992.

(39) Guldi, D. M. *Chem. Commun.* **2000**, 321.

(40) Polese, A.; Mondini, S.; Bianco, A.; Toniolo, C.; Scorrano, G.; Guldi, D. M.; Maggini, M. *J. Am. Chem. Soc*. **1999**, *121*, 3446.

(41) (a) Janssen, R. A. J.; Sariciftci, N. S.; Heeger, A. J. *J. Phys. Chem.* **1994**, *100*, 8641. (b) Peeters, E.; van Hal, P. A.; Knol, J.; Brabec, C. J.; Sariciftci, N. S.; Hummelen, J. C.; Janssen, R. A. J. *J. Phys. Chem. B* **2000**, *104*, 10174.

(42) Matsumoto, K.; Fujitsuka, M.; Sato, T.; Onodera, S.; Ito, O. *J. Phys. Chem. B* **2000**, *104*, 11632.

(43) (a) Marcus, R. A. *J. Chem. Phys.* **1956**, *24*, 966. (b) Marcus, R. A. *J. Chem. Phys.* **1957**, *26*, 867. (c) Marcus, R. A. *J. Chem. Phys.* **1957**, *26*, 872. (d) Marcus, R. A. *J. Chem. Phys.* **1965**, *43*, 679. (e) Marcus, R. A.; Sutin, N. *Biochim. Biophys. Acta* **1985**, *811*, 265.

(44) Ikemoto, J.; Takimiya, K.; Aso, Y.; Otsubo, T.; Fujitsuka, M.; Ito, O. *Org. Lett.* **2002**, *4*, 309.

(45) Gaines, G. L.; O'Neil, M. P.; Svec, W. A.; Niemczyk, M. P.; Wasielewski, M. R. *J. Am. Chem. Soc.* **1991**, *113*, 719.

(46) Weller, A. *Z. Phys. Chem.* **1982**, *132*, 93.

(47) (a) Förster, T. *Natuwissenschaften* **1946**, *33*, 166. (b) Förster, T. *Ann. Phys. (Leipzig)* **1948**, *2*, 55.

(48) Förster, T. Excitation Transfer. In *Comparative Effects of Radiation*; Burton, M., Kirby-Smith, J., Magee, J., Eds.; John Wiley & Sons: New York, 1960; p 300.

(49) Calvert, J. G.; Pitts, J. N., Jr. *Photochemistry*; John Wiley & Sons: New York, 1967; p 339.
(50) Dexter, D. L. *J. Chem. Phys.* **1953**, *21*, 836.
(51) Gasyna, Z.; Browett, W. R.; Stillman, M. J. *Inorg. Chem.* **1985**, *24*, 2440.
(52) Luo, C. P.; Fujitsuka, M.; Watanabe, A.; Ito, O.; Gan, L.; Huang, Y.; Huang, C. H. *J. Chem. Soc., Faraday Trans.* **1998**, *84*, 527.
(53) (a) Leland, B. A.; Joran, A. D.; Felker, P. M.; Hopfield, J. J.; Zewail, A. H.; Dervan, P. B. *J. Phys. Chem.* **1985**, *89*, 5571. (b) Oevering, H.; Paddon-Row, M. N.; Heppener, M. H.; Oliver, A. M.; Cotsaris, E.; Verhoeven, J. W.; Hush, N. S. *J. Am. Chem. Soc.* **1987**, *109*, 3258. (c) Johnson M. D.; Miller, J. R.; Green, N. S.; Closs, G. L. *J. Phys. Chem.* **1989**, *93*, 1173. (d) Finklea, H. O.; Hanshew, D. D. *J. Am. Chem. Soc.* **1992**, *114*, 3173.
(54) Osuka, A.; Maruyama, K.; Mataga, N.; Ashahi, T.; Yamazaki, I.; Tamai, N. *J. Am. Chem. Soc.* **1990**, *112*, 4958.
(55) Osuka, A.; Tanabe, S.; Kawabata, S.; Yamazaki, I.; Nishimura, Y. *J. Org. Chem.* **1996**, *60*, 7177.
(56) Grosshenny, V.; Harriman, A.; Ziessel, R. *Angew. Chem., Int. Ed. Engl.* **1955**, *34*, 1100.
(57) Becker, R. S.; de Melo, J. S.; Maçanita, A. L.; Elisei, F. *J. Phys. Chem.* **1996**, *100*, 18683.
(58) (a) Fujitsuka, M.; Ito, O.; Imahori, H.; Yamada, K.; Yamada, H.; Sakata, Y. *Chem. Lett.* **1999**, 721. (b) Konishi, T.; Fujitsuka, M.; Ito, O. *Chem. Lett.* **2000**, 202.
(59) (a) Brocks, G. *Synth. Met.* **1999**, *102*, 914. (b) Moro, G.; Scalmani, G.; Cosentio, U.; Pitea, D. *Synth. Met.* **1998**, *98*, 69. (c) Moro, G.; Scalmani, G.; Cosentio, U.; Pitea, D. *Synth. Met.* **2000**, *108*, 165. (d) Telesca, R.; Bolink, H.; Yunoki, S.; Hadziioannou, G.; Van Doijnnen P. Th.; Snijders, J. G.; Jonkman, H. T.; Sawatzky, G. A. *Phys. Rev. B* **2001**, *63*, 155112. (e) Geskin, V. M.; Dkhissi, A.; Brèdas, J. L. *Int. J. Quantum Chem.* **2003**, *91*, 350.